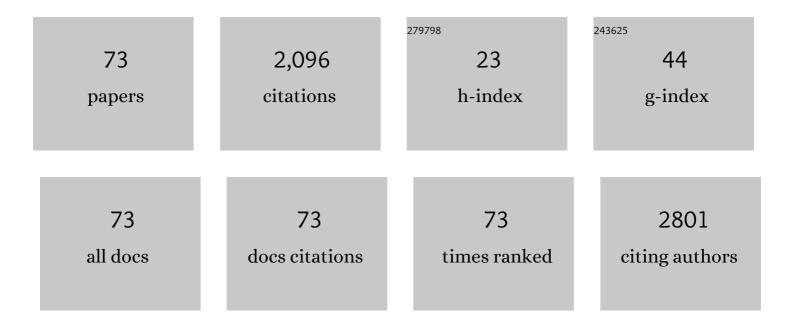
Li-Zhe Liu

List of Publications by Year in descending order

Source: https://exaly.com/author-pdf/53206/publications.pdf Version: 2024-02-01



Li.7ueliu

#	Article	IF	CITATIONS
1	Reaction kinetic acceleration induced by atomic-hybridized channels in carbon quantum dot/ReS2 composites for efficient Cr(VI) reduction. Applied Catalysis B: Environmental, 2022, 300, 119807.	20.2	15
2	Electronic structure transformation induced by dual-metal orbital hybridization in RexMn1-xS2 monolayer for hydrogen evolution reaction. Surfaces and Interfaces, 2022, 28, 101671.	3.0	1
3	Electronic reconfiguration induced by neighboring exchange interaction at double perovskite oxide interface for highly efficient oxygen evolution reaction. Chemical Engineering Journal, 2022, 432, 134330.	12.7	15
4	Multi-electron-channel integration to accelerate photogenerated carrier reaction kinetics for efficient sulfadiazine degradation. Applied Catalysis A: General, 2022, 633, 118513.	4.3	3
5	Electronic reconfiguration in layered Bi2SeO2 surface induced by dual-metal hybridization for hydrogen evolution reaction. Surfaces and Interfaces, 2022, 29, 101779.	3.0	1
6	The exchange between anions and cations induced by coupled plasma and thermal annealing treatment for room-temperature ferromagnetism. Physical Chemistry Chemical Physics, 2022, 24, 7001-7006.	2.8	3
7	Orbital Hybridization Induced by Doubleâ€Anion Coordination to Enhance Roomâ€Temperature Ferromagnetic Response. Physica Status Solidi - Rapid Research Letters, 2022, 16, .	2.4	0
8	Polarization-induced efficient charge separation in an electromagnetic coupling MOF for enhancing CO2 photocatalytic reduction. Journal of Colloid and Interface Science, 2022, 622, 402-409.	9.4	12
9	Spin-related symmetry breaking induced by half-disordered hybridization in BixEr2-xRu2O7 pyrochlores for acidic oxygen evolution. Nature Communications, 2022, 13, .	12.8	66
10	Photoluminescence and magnetism integrated multifunctional black phosphorus probes through controllable Pĩ€O bond orbital hybridization. Physical Chemistry Chemical Physics, 2021, 23, 22476-22482.	2.8	1
11	Recharged Catalyst with Memristive Nitrogen Reduction Activity through Learning Networks of Spiking Neurons. Journal of the American Chemical Society, 2021, 143, 5378-5385.	13.7	56
12	Superficial state regulation in double-anion-coupled Ni nanostructure for efficient hydrogen evolution reaction. Journal Physics D: Applied Physics, 2021, 54, 285502.	2.8	3
13	Spin-state reconfiguration induced by alternating magnetic field for efficient oxygen evolution reaction. Nature Communications, 2021, 12, 4827.	12.8	147
14	Strong histamine torsion Raman spectrum enables direct, rapid, and ultrasensitive detection of allergic diseases. IScience, 2021, 24, 103384.	4.1	5
15	Defect-engineering-enhanced electrical manipulation of anisotropic excitons in two-dimensional ReS2. Surfaces and Interfaces, 2021, 27, 101562.	3.0	4
16	Enhancing hydrogen evolution reaction by strain engineering in free-standing doped FeS monolayer. Materials Chemistry and Physics, 2020, 239, 122046.	4.0	6
17	Charged excited state induced by ultrathin nanotip drives highly efficient hydrogen evolution. Applied Catalysis B: Environmental, 2020, 262, 118305.	20.2	20
18	Resorcinarene Induced Assembly of Carotene and Lutein into Hierarchical Superstructures. Journal of the American Chemical Society, 2020, 142, 20583-20587.	13.7	19

LI-ZHE LIU

#	Article	IF	CITATIONS
19	Self-Assembly of Porphyrin-Based Metallacages into Octahedra. Journal of the American Chemical Society, 2020, 142, 17903-17907.	13.7	37
20	Lightâ€Controlled Ferromagnetism in Porphyrin Functionalized Ultrathin FeS Nanosheets. Advanced Optical Materials, 2020, 8, 2000046.	7.3	6
21	Dual-metal-driven Selective Pathway of Nitrogen Reduction in Orderly Atomic-hybridized Re ₂ MnS ₆ Ultrathin Nanosheets. Nano Letters, 2020, 20, 4960-4967.	9.1	69
22	Constructing Asymmetrical Ni-Centered {NiN ₂ O ₄ } Octahedra in Layered Metal–Organic Structures for Near-Room-Temperature Single-Phase Magnetoelectricity. Journal of the American Chemical Society, 2020, 142, 12841-12849.	13.7	7
23	Anchoring Black Phosphorus Nanoparticles onto ZnS Porous Nanosheets: Efficient Photocatalyst Design and Charge Carrier Dynamics. ACS Applied Materials & Interfaces, 2020, 12, 8157-8167.	8.0	53
24	Prediction of room-temperature multiferroicity in strained MoCr2S6 monolayer. Journal of Applied Physics, 2020, 127, 155302.	2.5	4
25	Electric Strain in Dual Metal Janus Nanosheets Induces Structural Phase Transition for Efficient Hydrogen Evolution. Joule, 2019, 3, 2955-2967.	24.0	75
26	Photoinduced semiconductor-metal transition in ultrathin troilite FeS nanosheets to trigger efficient hydrogen evolution. Nature Communications, 2019, 10, 399.	12.8	133
27	Stimulus-responsive electrochemiluminescence from self-assembled block copolymer and nonpolar carbon quantum dot composite nanospheres. Carbon, 2019, 147, 532-539.	10.3	9
28	Distorted Monolayer ReS ₂ with Low-Magnetic-Field Controlled Magnetoelectricity. ACS Nano, 2019, 13, 2334-2340.	14.6	14
29	Electronic structure and the hydrogen evolution reaction in layered ReS2 regulated by alkali-metal atom intercalation. Journal Physics D: Applied Physics, 2019, 52, 165301.	2.8	3
30	Selective and high-sensitive label-free detection of ascorbic acid by carbon nitride quantum dots with intense fluorescence from lone pair states. Talanta, 2019, 196, 530-536.	5.5	23
31	High-efficiency hydrogen evolution from seawater using hetero-structured T/Td phase ReS2 nanosheets with cationic vacancies. Nano Energy, 2019, 55, 42-48.	16.0	102
32	Ferromagnetism regulated by edged cutting and optical identification in monolayer PtSe2 nanoribbons. Journal Physics D: Applied Physics, 2018, 51, 225007.	2.8	10
33	Engineering the carrier dynamics of g-C ₃ N ₄ by rolling up planar sheets into nanotubes <i>via</i> ultrasonic cavitation. Nanoscale, 2018, 10, 22448-22455.	5.6	7
34	Oxygen-defect-dependent ferromagnetism and strain modulation in free-standing two-dimensional TiO ₂ monolayers. Physical Chemistry Chemical Physics, 2018, 20, 27176-27184.	2.8	7
35	Nonpolar-Oriented Wurtzite InP Nanowires with Electron Mobility Approaching the Theoretical Limit. ACS Nano, 2018, 12, 10410-10418.	14.6	30
36	Half-metallic carbon nitride nanosheets with micro grid mode resonance structure for efficient photocatalytic hydrogen evolution. Nature Communications, 2018, 9, 3366.	12.8	219

LI-ZHE LIU

#	Article	IF	CITATIONS
37	Highly Efficient Solarâ€Driven Photothermal Performance in Auâ€Carbon Coreâ€Shell Nanospheres. Solar Rrl, 2017, 1, 1600032.	5.8	24
38	Ultrahigh quantum efficiency photodetector and ultrafast reversible surface wettability transition of square In2O3 nanowires. Nano Research, 2017, 10, 2772-2781.	10.4	27
39	Phase-Engineering-Induced Generation and Control of Highly Anisotropic and Robust Excitons in Few-Layer ReS ₂ . Journal of Physical Chemistry Letters, 2017, 8, 2719-2724.	4.6	24
40	Complementary Metal Oxide Semiconductor-Compatible, High-Mobility, âŸ 111⟩-Oriented GaSb Nanowires Enabled by Vapor–Solid–Solid Chemical Vapor Deposition. ACS Nano, 2017, 11, 4237-4246.	14.6	38
41	Enhancement of Ferromagnetism in Nonmagnetic Metal Oxide Nanoparticles by Facet Engineering. Small, 2017, 13, 1602951.	10.0	12
42	Identification of Lattice Oxygen in Few-Layer Black Phosphorous Exfoliated in Ultrahigh Vacuum and Largely Improved Ambipolar Field-Effect Mobilities by Hydrogenation and Phosphorization. ACS Applied Materials & Interfaces, 2017, 9, 39804-39811.	8.0	10
43	Identification of nasopharyngeal carcinoma from photoluminescence spectra of 3C-SiC nanocrystals. Journal of Applied Physics, 2017, 122, 124702.	2.5	2
44	Electronic coupling between sulfur adsorption and oxygen vacancy in TiO ₂ microstructures for room-temperature ferromagnetism. Journal Physics D: Applied Physics, 2017, 50, 365304.	2.8	3
45	Regulation of oxygen vacancy types on SnO2 (110) surface by external strain. AIP Advances, 2016, 6, 055102.	1.3	3
46	Optical Identification of Topological Defect Types in Monolayer Arsenene by First-Principles Calculation. Journal of Physical Chemistry C, 2016, 120, 24917-24924.	3.1	24
47	Quantum confinement effects across two-dimensional planes in MoS2 quantum dots. Applied Physics Letters, 2015, 106, .	3.3	180
48	Electronic structure and magnetism in <i>g</i> -C4N3 controlled by strain engineering. Applied Physics Letters, 2015, 106, .	3.3	23
49	3C-SiC/ZnS heterostructured nanospheres with high photocatalytic activity and enhancement mechanism. AIP Advances, 2015, 5, .	1.3	6
50	Cubic In ₂ O ₃ Microparticles for Efficient Photoelectrochemical Oxygen Evolution. Journal of Physical Chemistry Letters, 2014, 5, 4298-4304.	4.6	49
51	3C-SiC nanocrystals/TiO2 nanotube heterostructures with enhanced photocatalytic performance. Applied Physics Letters, 2014, 104, .	3.3	11
52	Enhanced fluorescence from dye molecules by Au nanoparticles on asymmetric double-stranded DNA and mechanism. Applied Physics Letters, 2014, 104, .	3.3	5
53	Dopant-Induced Surface Magnetism in β-SiC Controlled by Dopant Depth. Journal of Physical Chemistry C, 2014, 118, 25429-25433.	3.1	7
54	Optical identification of oxygen vacancy types in SnO2 nanocrystals. Applied Physics Letters, 2013, 102, .	3.3	65

LI-ZHE LIU

#	Article	IF	CITATIONS
55	Resonant Raman scattering from CdS nanocrystals enhanced by interstitial Mn. Applied Physics Letters, 2013, 102, .	3.3	24
56	Electronic structure and optical properties of β-FeSi2(100)/Si(001) interface at high pressure. Applied Physics Letters, 2012, 101, 111909.	3.3	2
57	Oxygen-vacancy and depth-dependent violet double-peak photoluminescence from ultrathin cuboid SnO2 nanocrystals. Applied Physics Letters, 2012, 100, 121903.	3.3	45
58	ldentification of oxygen vacancy types from Raman spectra of SnO ₂ nanocrystals. Journal of Raman Spectroscopy, 2012, 43, 1423-1426.	2.5	172
59	Electronic states and photoluminescence of TiO2 nanotubes with adsorbed surface oxygen. Applied Physics Letters, 2012, 100, 121904.	3.3	17
60	Si–Si optical phonon behavior in localized Si clusters ofÂSi x Ge1â^'x ÂalloyÂnanocrystals. Applied Physics A: Materials Science and Processing, 2011, 103, 361-365.	2.3	4
61	Surface carbon layer and visible-light photocatalytic activities of carbon-coated TiO 2 nanotubes synthesized in organic electrolytes. Applied Physics A: Materials Science and Processing, 2011, 105, 703-707.	2.3	7
62	Growth of tin oxide nanorods induced by nanocube-oriented coalescence mechanism. Applied Physics Letters, 2011, 98, 133102.	3.3	21
63	Morphology-dependent low-frequency Raman scattering in ultrathin spherical, cubic, and cuboid SnO2 nanocrystals. Applied Physics Letters, 2011, 99, 251902.	3.3	7
64	Twinning Ge0.54Si0.46 nanocrystal growth mechanism in amorphous SiO2 films. Applied Physics Letters, 2010, 96, .	3.3	13
65	Crystalline Core/Shell Si/SiO ₂ Nanotubes Formed via Interfacial Stress Imbalance. Journal of Nanoscience and Nanotechnology, 2010, 10, 5583-5586.	0.9	1
66	Size-independent low-frequency Raman scattering in Ge-nanocrystal-embedded SiO_2 films. Optics Letters, 2010, 35, 1022.	3.3	9
67	Longitudinal optical phonon–plasmon coupling in luminescent 3C–SiC nanocrystal films. Optics Letters, 2010, 35, 4024.	3.3	15
68	Photoluminescence from colloids containing aluminum hydroxide nanocrystals with uniform size. Applied Physics Letters, 2010, 97, 121901.	3.3	10
69	Identification of local silicon cluster nanostructures inside SixGe1â^'x alloy nanocrystals by Raman spectroscopy. Chemical Communications, 2010, 46, 5539.	4.1	13
70	Ordered amorphous silicon nanoisland arrays and reflection spectral dependence on nanoisland geometrical parameters. Applied Physics Letters, 2009, 94, 151903.	3.3	8
71	Raman investigation of oxidation mechanism of silicon nanowires. Applied Physics Letters, 2009, 95, .	3.3	14
72	Surface-polarization-induced formation of amorphous foliaceous SiO2 helical nanobelts. Applied Physics Letters, 2009, 94, 253110.	3.3	5

#	Article	IF	CITATIONS
73	Influence of GeSi interfacial layer on Ge–Ge optical phonon mode in SiO2 films embedded with Ge nanocrystals. Applied Physics Letters, 2009, 95, .	3.3	11